Development of a PET/CT Molecular Radiomics-clinical Model to Predict Local Lymph Node Metastasis of Invasive Lung Adenocarcinoma (≤ 3cm)

Cheng Chang
Shanghai Chest Hospital: Shanghai Jiao Tong University Affiliated Chest Hospital
Maomei Ruan
Shanghai Chest Hospital: Shanghai Jiao Tong University Affiliated Chest Hospital
Chunji Chen
Shanghai Chest Hospital: Shanghai Jiao Tong University Affiliated Chest Hospital
Hong Yu
Shanghai Chest Hospital: Shanghai Jiao Tong University Affiliated Chest Hospital
Xiaoyan Sun
Shanghai Chest Hospital: Shanghai Jiao Tong University Affiliated Chest Hospital
Yaqiong Ge
GE Healthcare
Shaofeng Duan
GE Healthcare
Wenjing Teng
Shanghai University of Traditional Chinese Medicine
Qianfu Wu
Shanghai University of Traditional Chinese Medicine
Wenlu Zhao
Second Affiliated Hospital of Soochow University
Xiaohua Qian
Shanghai Jiao Tong University School of Biomedical Engineering
Rui Wang
Shanghai Chest Hospital: Shanghai Jiao Tong University Affiliated Chest Hospital
Bei Lei
Shanghai Chest Hospital: Shanghai Jiao Tong University Affiliated Chest Hospital
Lihua Wang
Shanghai Chest Hospital: Shanghai Jiao Tong University Affiliated Chest Hospital
Hui Yan
Shanghai Chest Hospital: Shanghai Jiao Tong University Affiliated Chest Hospital

Ciyi Liu
Shanghai Chest Hospital: Shanghai Jiao Tong University Affiliated Chest Hospital
Liu Liu
Shanghai Chest Hospital: Shanghai Jiao Tong University Affiliated Chest Hospital
Jian Feng
Shanghai Chest Hospital: Shanghai Jiao Tong University Affiliated Chest Hospital
Wenhui Xie (xknuclear@163.com)
Shanghai Chest Hospital Shanghai Jiao Tong University https://orcid.org/0000-0003-1294-4554

Research Article

Keywords: CT, PET/CT, Radiomics, Lymph node metastasis, Lung adenocarcinoma

Posted Date: May 17th, 2021

DOI: https://doi.org/10.21203/rs.3.rs-520429/v1

Abstract

Purpose To investigate the value of ^{18}F-FDG PET/CT molecular radiomics combined with the clinical model in predicting local lymph node metastasis (LLNM) with invasive lung adenocarcinoma (≤3cm).

Methods 528 lung adenocarcinoma patients were enrolled in this retrospective study. Five models, including integrated PET/CT molecular radiomics-clinical, PET/CT radiomics, PET radiomics, CT radiomics, and clinical models, were developed for the prediction of LLNM. The predictive performance was examined by ROC curve analysis and clinical utility was validated by nomogram and decision curve analysis (DCA) analyses.

Results 10 PET/CT radiomics features and 2 clinical characteristics were selected for the construction of the integrated PET/CT molecular radiomics-clinical model. This integrated model performed better than the clinical model and three other radiomics models, and the AUC value of the integrated model was 0.95 (95% CI: 0.93-0.97) in the training group and 0.94 (95% CI: 0.89-0.97) in the test group, respectively. The clinical application of this integrated model in predicting LLNM was also confirmed by nomogram and DCA analyses.

Conclusions The integrated PET/CT molecular radiomic-clinical model developed here has the greater advantage to predict LLNM of clinical invasive lung adenocarcinoma (≤3cm) when compared with the simple radiomics model or clinical model.

Introduction

Lung adenocarcinoma accounts for over 30% of all lung cancers. Notably, some invasive lung adenocarcinoma (≤3cm) is already accompanied by lymph node metastasis(LNM)at the time of diagnosis [1]. To determine whether there is local lymph node metastasis (LLNM) before the operation can not only avoid an unnecessary radical operation, but also guide intraoperative mediastinal lymph node dissection to achieve the purpose of radical resection in some invasive lung adenocarcinoma (≤ 3cm) [1]. Besides, determining lymph node metastasis status before radiotherapy is also important for the selection of the target range of radiotherapy [2]. Although thoracoscopy and transbronchial biopsies have high accuracy for the detection of LLNM, they will bring certain trauma to the patients and increase treatment costs [3]. Positron emission tomography/computed tomography (PET/CT) is considered to be the most accurate LLNM staging method, but its diagnostic sensitivity and specificity are still not high and affected by several factors [4–6]. For example, the diameter of some micro-metastasis of lymph nodes is smaller than the spatial resolution range of PET/CT, which may cause false negatives [7]. Also, long-term smoking and lung infections can cause false positives [8]. Besides, PET/CT image reading is highly subjective, heavily dependent on doctors' experience. The accuracy of PET/CT in predicting the incidence of occult LNM in non-small cell lung cancer is only about 14–19% [9, 10].

Radiomics can help improve the diagnostic efficiency of lung cancer lymph node metastasis [11]. Coroller et al. reported that 35 CT radiomics features of lung adenocarcinoma can be used to predict distant

metastasis [12]. Yang et al. demonstrated that CT radiomics can be used to predict lung adenocarcinoma lymph node metastasis [13]. Cong et al. used the random forest method to establish models and predict the lymph node metastasis of lung adenocarcinoma [14]. Although CT-based radiomics feature evaluation application has been proven to be used to predict lung adenocarcinoma lymph node metastasis, the PET/CT molecular radiomics-clinical model, including PET/CT molecular radiomics features and clinical factors, has not been investigated to predict LLNM in lung adenocarcinoma. Also, the comparative study of PET/CT, CT, PET radiomics models for predicting LLNM of lung adenocarcinoma has not seen studied. PET/CT radiomics delineates the primary lesions of PET and CT images, extracts and analyzes radiomics features, establishes models, and provides digital diagnostic information, which cannot be observed directly with naked eyes [15]. This study intends to analyze the features of PET/CT images of patients with lung adenocarcinoma, and explores the diagnostic efficacy of PET/CT, CT, and PET radiomics models in predicting LLNM of lung adenocarcinoma. Also, we aim to develop an integrated PET/CT molecular radiomics-clinical model to predict LLNM of invasive lung adenocarcinoma (≤ 3cm).

Materials And Methods

Patient selection

A retrospective analysis of 802 patients (802 cases) with lung adenocarcinoma (diameter ≤ 3 cm) was collected from the Shanghai Chest Hospital from February 2016 to January 2021, all tumors and lymph nodes (no less than 6 groups with N1 or N2 dissection) confirmed by pathological examination. The criteria of inclusion and exclusion are illustrated in Supplementary Figure S1.

Pathological evaluation

The pathological histology of all tumors was evaluated by two pathologists in lung tumors following 2015 WHO classification of lung adenocarcinoma. Lymph node staging was diagnosed according to the eighth version of the TNM staging method. The lymph node metastasis of lung adenocarcinoma was divided into 1 to 14 groups. N1 lymph nodes were located in the ipsilateral intrapulmonary or hilar lymph nodes (11–14 groups), and N2 lymph nodes were located in the ipsilateral mediastinal lymph nodes (2–9 groups).

Clinical information of selected lung adenocarcinoma

The clinical information of these patients collected here included age, gender, smoking history, tumor marker carcinoembryonic antigen (CEA). CT features included lung tumor location, lobulation sign, burr sign, pleural traction, and solid component size. PET parameter included SUVmax value. The clinical information of these enrolled cases was summarized in Table 1. The size of the solid component of pulmonary nodules, including mixed ground-glass nodules, referred to the average value of the longest cross-section length and vertical diameter length of the solid component on the pulmonary window [16].

Table 1
Clinical features of 528 patients enrolled in this study

Clinical characteristics	Training (n = 371)			Testing (n = 157)		
	Lymph node (-)	Lymph node (+)	P value	Lymph node (-)	Lymph node (+)	P value
Age,year (median;IQR)	62; 55 ~ 67	62; 55 ~ 68	0.62	63; 56 ~ 69	60; 50 ~ 70	0.166
Gender Male	103	46	0.369	48	23	0.555
Female	163	59		65	21	
Smoke Yes	84	36	0.617	38	15	0.958
No	182	69		75	29	
Location Upper lobe, right	109	30	0.024	48	12	0.101
Middle lobe, right	46	18		21	10	
Lower lobe, right	13	8		5	1	
Upper lobe, left	60	29		26	15	
Lower lobe, left	38	20		13	6	
CEA, ng/ml (median; IQR)	2.32; 1.53 ~ 3.93	3.67; 2.11 ~ 8.50	0.273	2.21; 1.53 ~ 3.52	3.59; 2.01 ~ 6.27	0.251
Lobulation (+)	260	103	0.836	112	44	0.279
(-)	6	2		1	0	
Burr (+)	249	102	0.176	112	44	0.688
(-)	17	3		1	0	
Pleural traction (+)	45	53	< 0.001	15	18	< 0.001
(-)	221	52		98	26	
Solid components, cm (median; IQR)	0.85; 0.50 ~ 1.3	2.05; 1.65 ~ 2.45	< 0.001	0.95; 0.55 ~ 1.4	2.1; 1.65 ~ 2.49	< 0.001
SUVmax (median;IQR)	3.68; 2.1 ~ 7.45	11.11; 8.92 ~ 15.31	0.145	3.57; 2.08 ~ 6.99	10.25; 7.1 ~ 13.36	0.279

PET/CT scan procedures

All patients were examined under the same scanning conditions on the same device (Siemens Biograph MCT-S PET/CT). CT was a 64-slice spiral CT. ^{18}F-FDG is provided by Shanghai Atom Kexing

Pharmaceuticals Co., Ltd. All patients were forbidden to eat and drink for more than 6 hours before PET/CT, with blood sugar below 150mg/ dL. All patients were injected with ^{18}F-FDG at 5 mBq/kg ± 10% of body weight and then rested for 60 minutes. The PET scan was divided into 5 or 6 beds, each bed was checked for about 2 minutes. CT data were used to attenuate correction PET images, and Truex + TOF was used to reconstruct PET images. The PET and CT scan thickness of all patients was 5mm. The matrix size of all PET reconstruction was 200 × 200, and the anisotropic voxel was 4.07 × 4.07 × 3.0 mm^3. After regular PET and CT image scans, 1 mm breath-hold lung CT scan was added. CT was reconstructed by conventional algorithm, PET was reconstructed by iterative method.

PET/CT image processing and analysis

The 5 mm PET and 1 mm CT images of all patients were exported from PACS workstation in DICOM format, and then imported into ITK-SNAP software (version 3.8.0-beta, www.itksnap.org)to outline lung cancer in 3D mode. The entire delineation was completed by two medical imaging doctors with a history of not less than 12 years, and none of them knew the patient's pathological results. For CT image delineation, we observe the lesion on the lung window (window width 1600Hu, window level − 600Hu).

The two doctors delineated the primary tumor on PET images, using a 40% SUVmax threshold to characterize the volume of interest (VOI) [17–21]. To avoid including the physiologic uptake in the VOI, a combined CT and PET scan reading is performed [19–21]. An example of VOI delineation is shown in Fig. 1.

Image pre-processing

The original 5mm PET, 1mm breath-holding thin-layer CT (DICOM format), and the outlined VOI of each lung tumor were inputted into IBSI-compatible Artificial Intelligence Kit software (AK analysis kit, GE healthcare, 3.2.2) to be preprocessed [20–24]. The μ ± 3σ method was used to remove data with the brightness greater than 3σ to normalize the image brightness [20, 21, 25]. The images were resampled to 1 x 1 x 1 mm^3 by using Linear interpolation to improve the resolution of the images. The pre-processed images were imported into ITK-SNAP to delineated the VOI.

Segmentation, feature extraction, feature selection, radiomic model construction, and validation

The intra- and inter-observer consistency coefficients were evaluated, 50 cases were randomly selected from the enrolled study cases. Two observers (observer A and B) with more than 10 years of experience in PET and CT applications delineated the VOIs. Observer A delineated the VOI of CT and PET images twice at an interval of 4 weeks, and the intra- observer consistency coefficients of the extracted features were evaluated between the two delineations of observer A. Observer B delineated the VOI independently once, and the inter-observer consistency coefficients between the radiomics feature extracted by the observer A (first time) and B and were evaluated. ICC > 0.75 indicates good agreement. Observer A finished the rest delineation. Based on the VOI of lung tumors outlined by observer A from CT and PET images, 402 radiomics features were extracted in every image by using AK software, including 42 histograms, 154

gray level co-occurrence matrix (GLCM), 15 formfactors features that described the shape of the VOI, 180 run length matrix (RLM) features and 11 gray level size zone matrix (GLSZM) features. The bin width was set to 25 while extracting the features.

The patients were randomly assigned into training (371 cases) and test group (157 cases) according to the ratio of 7:3 by using a stratified sampling method to ensure the balance of positive and negative samples in the training group and test group [17, 20–25]. In the training set minimum redundancy and maximum correlation (mRMR) and least absolute shrinkage and selection operator (LASSO) methods were used to select the most valuable radiomics features for predicting lung adenocarcinoma lymph node metastasis based on the features with ICC > 0.75. Then three multivariate logistic regression models based on PET/CT, CT, and PET were established in the training group.

The radiomic score of each patient was calculated based on the combination of the retained features weighted by LASSO logistic regression coefficients (Supplementary Methods). The area under the curve (AUC) was used to evaluate the diagnostic efficacy of the three-group radiomics model in predicting LLNM of lung adenocarcinoma. The efficacy of predicting LLNM of lung adenocarcinoma was evaluated in the test group. Delong test was employed to compare the performance of the three different models based on PET/CT, CT, and PET to figure out the most predictive model. To verify the reliability of the model, 100 times repeated cross-validation was performed. The workflow of radiomic analysis is shown in Fig. 1.

Construction of the radiomic nomogram

The univariate analysis was applied to clinical factors, factors with $p < 0.1$ were analyzed by using univariate logistic regression to identify whether the features were discriminative ($p < 0.05$) between the groups. Then multivariate logistic regression was applied to these discriminative clinical features to construct a clinical model, also the clinical features, as well as the radiomics score, were integrated to establish a predictive nomogram. Moreover, variance inflation factor (VIF) was used for collinearity analysis, and the factors with VIF > 10 were eliminated. All models were constructed in the training group and then validated in the test group.

Statistical analysis

In this study, R language software (version 3.5.1) was used for statistical analysis. For clinical data, the chi-square test was applied to normal distribution features which were given as mean ± sd, wilcoxon test was applied to abnormal distributions, and which were given as median (lower quartile, upper quartile). Decision curve analysis (DCA) was used to evaluate the clinical utility of the PET/CT molecular radiomics-clinical model in the test group to predict lung adenocarcinoma lymph node metastasis.

Results

Enrollment of patients

528 lung adenocarcinoma patients were included in this study, including 149 patients with LLNM (37 with N1 involvement, 112 with N2 involvement) and 379 patients without LLNM (Table 1).

Radiomic features extraction and selection from PET/CT images

For the radiomics features extracted twice by observer A, the intra-ICC range in the CT group, PET group were 0.06-1 and 0.32-1. For the features extracted by observer A (first time) and observer B, the inter-ICC range in CT groups and PET group were 0.15-1 and 0.3-1, the features with ICC > 0.75 in both intra- and inter-group were retained for further analysis (Supplementary Table S1). Data sets of PET/CT, CT, and PET data were further analyzed by the mRMR and LASSO regression models. After feature extraction and selection, 10 PET/CT (6 CT and 4 PET), 12 CT, and 10 PET radiomic features were retained, the feature name and their corresponding coefficients were shown in Supplementary Figure S2-4.

Evaluation of the performance of three radiomic models

The results showed that all three models (PET/CT, CT, and PET) can predict the lymph node metastasis, the cutoff values were − 0.66, -0.75, -0.13 respectively (Supplementary Figure S2C, S3C, S4C). To prove the stability of the model, 100 times repeated cross-validation was performed (Supplementary Figure S2D). The AUC values of the PET/CT, CT, PET radiomics models in the training group were 0.92 (95% CI: 0.89–0.95), 0.87 (95% CI: 0.83–0.90), 0.83 (95% CI: 0.78–0.86), respectively; The AUC values of three models in the test group were 0.91 (95% CI: 0.86–0.95), 0.87 (95% CI: 0.80–0.92), 0.80 (95% CI: 0.73–0.86), respectively (Fig. 2). The sensitivity, specificity, and accuracy of PET/CT, CT, PET radiomics models for predicting LLNM of lung adenocarcinoma in the training and test group were also summarized in Table 2. The Delong test showed that the performance of the PET/CT model is much better than PET or CT models ($p < 0.05$) in the training group (Table 3).

Table 2
The performance of 5 different models for prediction of lymph metastasis of lung adenocarcinoma

Models	AUC (95% CI)	ACC (95% CI)	SEN	SPE	PPV	NPV
Training group						
PET/CT	0.92 (0.89–0.95)	0.865(0.826–0.898)	0.865	0.867	0.943	0.717
CT	0.87 (0.83–0.90)	0.741(0.694–0.785)	0.688	0.876	0.934	0.526
PET	0.83 (0.78–0.86)	0.765(0.719–0.808)	0.759	0.781	0.898	0.562
Clinical	0.93 (0.90–0.95)	0.838(0.797–0.974)	0.664	0.94	0.867	0.827
PET/CT + Clinical	0.95 (0.93–0.97)	0.879(0.841–0.91)	0.717	0.974	0.943	0.853
Test group						
PET/CT	0.91 (0.86–0.95)	0.873(0.81–0.92)	0.885	0.841	0.935	0.74
CT	0.87 (0.80–0.92)	0.771(0.697–0.834)-	0.717	0.909	0.953	0.556
PET	0.80 (0.73–0.86)	0.79(0.718–0.851)	0.832	0.682	0.87	0.612
Clinical	0.91 (0.85–0.95)	0.783(0.711–0.845)	0.578	0.925	0.841	0.761
PET/CT + Clinical	0.94 (0.89–0.97)	0.847(0.781–0.89)	0.656	0.978	0.955	0.805

AUC: area under the curve; CI: confidence interval; ACC: accuracy; SEN: sensitivity; SPE: specificity; PPV: positive predictive value; NPV: negative predictive value.

Table 3
DeLong test of ROC curves between different models

Comparisons	Training		Testing	
	Z score	p value	Z score	p value
PET/CT vs. PET model	5.157	< 0.001	3.653	< 0.001
PET/CT vs. CT model	3.514	< 0.001	1.931	0.054
PET vs. CT model	1.299	0.194	1.35	0.177
Integrated vs. PET/CT model	3.943	< 0.001	1.65	0.099
Integrated vs. Clinical model	3.257	< 0.001	2.011	0.044
PET/CT vs. Clinical model	0.484	0.628	0.268	0.788

Development of a clinical model to predict LLNM of lung adenocarcinoma

We further took steps to establish a clinical model to predict LLNM of lung adenocarcinoma. After screening of clinical models, we found that clinical characteristics, including pleural traction, size of solid components, and locations, were statistically significant in predicting LLNM by univariate logistic analysis of clinical features in the training group (Table 4). By multivariate logistic regression analysis, the results showed the size of solid components and the location of the lesion were independent predictors ($p < 0.05$) for predicting lymph node metastasis of lung adenocarcinoma, as shown in Table 5. The AUC value of the clinical model in the training and test group was 0.93 (95% CI: 0.90–0.95), 0.91 (95% CI: 0.85–0.95), respectively (Table 2).

Table 4
Univariate logistic analysis of clinical features and lymph node metastasis

Variables	OR	P value
Pleural traction	5.01(3.05–8.29)	< 0.001
Solid composition	37.99(18.69–87.63)	< 0.001
Locations	1.18(1.02–1.36)	0.027

Table 5
Multivariate logistic analysis of clinical and radiomic features and lymph node metastasis

Variables	OR	P value
Solid composition	13.32(5.92–33.61)	< 0.001
Locations	1.28(1.01–1.63)	0.044
Radscore	2.04(1.55–2.78)	< 0.001
Intercept	0.01(0-0.04)	< 0.001

Construction of an integrated PET/CT molecular radiomics-clinical model to predict LLNM of lung adenocarcinoma

The integrated PET/CT molecular radiomics-clinical logistic regression model was constructed by using the radiomic score and two independent clinical risk factors and the results were shown as the nomogram (Fig. 3A). In both the training set and test group, the PET/CT molecular radiomics-clinical model showed good power to predict lymph node metastasis (Table 2). The AUC values of the training and test group were 0.95 (95% CI: 0.93–0.97) and 0.94 (95% CI: 0.89–0.97), respectively. The AUC values of PET/CT radiomics-clinical, PET/CT radiomics, and clinical factors models were compared by DeLong test. It was found that the performance of the PET/CT radiomics-clinical model was significantly better than PET/CT radiomic model or clinical model alone in the training group (Table 3). The calibration

curves of the nomogram were shown in Fig. 3B, which displayed a good calibration of the nomogram. Finally, we compared the clinical usefulness of these models by DCA. When the threshold probability of predicting lung adenocarcinoma lymph node metastasis is between 1–70%, the application of the PET/CT molecular radiomics-clinical model to predict LLNM of lung adenocarcinoma has greater advantages than the clinical model (Fig. 3C).

Discussion

Patients with occult LLNM of lung adenocarcinoma are likely to cause recurrence after surgery. Although CT has been routinely used to diagnose lymph node metastasis of lung cancer, it only observes tumor lesions based on morphological characteristics and thus has multiple limitations. PET/CT is a more accurate method for diagnosing local lymph node metastasis. For lymph nodes less than 1 cm, PET/CT has a greater advantage compared with CT. Upon intake of imaging reagent, metastatic lesions of lung adenocarcinoma can be judged from the perspective of molecular metabolism [4, 26]. However, there is subjectivity in predicting lymph node metastasis by PET/CT.

Many studies have demonstrated the value of CT radiomics in predicting lymph node metastasis of lung cancer (13,14). In this study, 10 radiomics features extracted from PET/CT images were demonstrated to have the ability to predict LLNM of lung adenocarcinoma. The AUC value of the ROC curve is 0.92 in the training set and 0.91 in the test set (Table 2). Notably, this study incorporates the size of solid components of lung adenocarcinoma into clinical factors, which is innovative and clinically practical. The integrated PET/CT molecular radiomic-clinical model constructed here by the use of clinical characteristics and radiomic features in terms of nomograms and clinical decision curves can help doctors to better predict the lymph node metastasis of lung adenocarcinoma.

There are several findings of this study. First, among the common clinical features of PET/CT, SUVmax is not significantly related to lymph node metastasis, which was in line with some previous studies. For example, Ouyang et al. found that SUVmax uptake in lung cancer was not an independent predictor of LLNM [27]. They attribute this to some of the inherent characteristics of SUVmax [28, 29]. It was susceptible to several uncontrolled sources of variation, such as uptake cycle length, blood glucose, and partial volume effect. However, other studies have shown that the SUVmax in lung cancer was an independent predictor of LLNM, so this issue still needs to be further discussed [30]. Second, the radiomic features of PET/CT images combined with clinical risk factors improve the diagnostic accuracy of predicting LLNM. Third, the nomogram generated here can provide a quantitative and intuitive method for clinicians to predict lymph node metastasis of lung adenocarcinoma. Lastly, it has been reported that there is a strong correlation between the diameter of solid components on CT images and the invasive components revealed by pathology, and the size of solid components is an important factor affecting prognosis. Here, we found that the solid proportion size can be used as an effective predictor of LLNM [31, 32].

This study has some limitations. Firstly, this study was a single-center retrospective study. Although some data have been extracted from the included cases as a validation set for evaluating radiomics models, a larger multi-center study is still needed to verify this study. Second, the segmentation of lung adenocarcinoma lesions is semi-automatically delineated by nuclear medicine doctors through ITK software, which is very time-consuming. We hope that with the development of artificial intelligence software such as deep learning, fully automatic computer segmentation can be realized [17, 33–34]. Finally, due to the short time after surgery and incomplete follow-up, no survival rate prediction model was established.

In conclusion, PET/CT molecular radiomics model has the high diagnostic value in predicting LLNM of lung adenocarcinoma. We developed a PET/CT molecular radiomics-clinical nomogram model as a visualization tool for patient prediction, providing the possibility of predicting LLNM for newly diagnosed lung adenocarcinoma patients.

Declarations

Funding information

This study was financially supported by the special project of integrated traditional Chinese and Western medicine in general hospital of Shanghai Health Committee (Grant Number ZHYY-ZXYJHZX-202023); the Natural Science Foundation of Shanghai (Grant Number 18ZR1435200); the Nurture projects for basic research of Shanghai Chest Hospital (Grant Number 2020YNJCM07); the National Natural Science Foundation of China (Grant Number 82071873);the National Natural Science Foundation of China (Grant Number 81871353); the Shanghai Sailing Program (grant numbers 20YF1444500); Nurture projects for basic research of Shanghai Chest Hospital (grant number 2020YNJCQ11); the Youth Medical Talents–Medical Imaging Practitioner Program (grant number SHWRS(2020)_087); the Shanghai Sailing Program (grant numbers 19YF445400); Shanghai university of traditional Chinese medicine budget project (18LK055); Nurture projects for basic research of Shanghai Chest Hospital (grant number 2020YNJCQ06); the National Natural Science Foundation of China (Grant Number 81773007), and the National Natural Science Foundation of China (Grant Number 81602415).

Authors' contributions

Cheng Chang, Maomei Ruan and Chunji Chen design and discussion of research methods and writing of the original manuscript. Wenhui Xie and Jian Feng designed the study. Xiaoyan Sun, Bei Lei, Lihua Wang, Liu Liu, Hui Yan, Ciyi Liu collected data. Yaqiong Ge, Shaofeng Duan made data statistics. Wenjing Teng, Hong Yu, Wenlu Zhao, Rui Wang designed of research methods. Xiaohua Qian designed of research methods in radiomics. All the authors read and approved the final manuscript.

Compliance with ethical standards

Conflict of interest

Two of the authors of this manuscript (Yaqiong Ge, Shaofeng Duan) are employees of GE Healthcare. The remaining authors declare that the research was conducted in the absence of any commercial or financial relationships that could be construed as a potential conflict of interest.

Ethical approval

All procedures performed in studies involving human participants were approved by the Institutional Review Board of Shanghai Jiao Tong University-affiliated Shanghai Chest Hospital and with the 1964 Helsinki declaration and its later amendments or comparable ethical standards. For this type of study formal consent is not required. This article does not contain any animal experiments.

References

1. Postmus PE, Kerr KM, Oudkerk M, Senan S, Waller DA, Vansteenkiste J, et al. Early and locally advanced non-small-cell lung cancer (NSCLC): ESMO Clinical Practice Guidelines for diagnosis, treatment and follow-up. Ann Oncol. 2017;28:iv1-iv21. doi:10.1093/annonc/mdx222.
2. Ramnath N, Dilling TJ, Harris LJ, Kim AW, Michaud GC, Balekian AA, et al. Treatment of stage IIl non-small cell lung cancer: Diagnosis and management of lung cancer, 3rd ed: American College of Chest Physicians evidence-based clinical practice guidelines. Chest. 2013;143:e314S-e40S. doi:10.1378/chest.12-2360.
3. Czarnecka-Kujawa K, Yasufuku K. The role of endobronchial ultrasound versusmediastinoscopy for non-small cell lung cancer. J Thorac Dis. 2017;9:S83-S97. doi:10.21037/jtd.2017.03.102.
4. Birim O, Kappetein AP, Stijnen T, Bogers AJJC. Meta-analysis of positron emission tomographic and computed tomographic imaging in detecting mediastinal lymph node metastases in nonsmall cell lung cancer. Ann Thorac Surg. 2005; 79(1): 375-82. doi: 10.1016/j.athoracsur.2004.06.041.
5. Gould MK, Kuschner WG, Rydzak CE, Maclean CC, Demas AN, Shigemitsu H, et al. Test performance of positron emission tomography and computed tomography for mediastinal staging in patients with non-small-cell lung cancer: a meta-analysis. Ann Intern Med. 2003;139(11):879-92. doi: 10.7326/0003-4819-139-11.200311180-00013.
6. Groheux D, Quere G, Blanc E, Lemarignier C, Vercellino L, de Margerie-Mellon C, et al. FDG PET-CT for solitary pulmonary nodule and lung cancer: Literature review. Diagn Interv Imaging. 2016;97:1003-17. doi:10.1016/j.diii.2016.06.020.
7. Liu Y. Role of FDG PET-CT in evaluation of locoregional nodal disease for initial staging of breast cancer. World J Clin Oncol. 2014; 5:982-9. doi:10.5306/ wjco. v5.i5.982.
8. Capitanio S, Nordin AJ, Noraini AR, Rossetti C. PET/CT in nononcological lung diseases: current applications and future perspectives. Eur Respir Rev. 2016;25:247-58. doi:10.1183/16000617.0051-2016.
9. Shimada Y, Tsuboi M, Saji H, Miyajima K, Usuda J, Uchida O, et al. The prognostic impact of main bronchial lymph node involvement in non-small cell lung carcinoma: suggestions for a modification

of the staging system. Ann Thorac Surg. 2009;88:1583-8. doi:10.1016/j.athoracsur.2009.04.065.

10. El-Sherief AH, Lau CT, Carter BW, Wu CC. Staging Lung Cancer: Regional Lymph Node Classification. Radiol Clin North Am. 2018;56:399-409. doi:10.1016/j.rcl.2018.01.008.
11. Zhu X, Dong D, Chen Z, Fang M, Zhang L, Song J, et al. Radiomic signature as a diagnostic factor for histologic subtype classification of non-small cell lung cancer. Eur Radiol. 2018;28:2772-8. doi:10.1007/s00330-017-5221-1.
12. Coroller TP, Grossmann P, Hou Y, Rios Velazquez E, Leijenaar RT, Hermann G, et al. CT-based radiomic signature predicts distant metastasis in lung adenocarcinoma. Radiother Oncol. 2015;114:345-50. doi:10.1016/j.radonc.2015.02.015.
13. Yang X, Pan X, Liu H, Gao D, He J, Liang W, et al. A new approach to predict lymph node metastasis in solid lung adenocarcinoma: a radiomics nomogram. J Thorac Dis. 2018;10:S807-S19. doi:10.21037/jtd.2018.03.126.
14. Cong M, Feng H, Ren JL, Xu Q, Cong L, Hou Z, et al. Development of a predictive radiomics model for lymph node metastases in pre-surgical CT-based stage IA non-small cell lung cancer. Lung Cancer. 2020;139:73-9. doi:10.1016/j.lungcan.2019.11.003.
15. Lambin P, Leijenaar RTH, Deist TM, Peerlings J, de Jong EEC, van Timmeren J, et al. Radiomics: the bridge between medical imaging and personalized medicine. Nat Rev Clin Oncol. 2017;14:749-62. doi:10.1038/nrclinonc.2017.141.
16. Chang C, Sun XY, Zhao WL,Wang R, Qian XH, Lei B, et al. Minor components of micropapillary and solid subtypes in lung invasive adenocarcinoma (≤ 3 cm): PET/CT findings and correlations with lymph node metastasis. Radiol Med. 2020;125:257-264. doi:10.1007/s11547-019-01112-x.
17. Bashir U, Azad G, Siddique MM, Dhillon S, Patel N, Bassett P, et al. The effects of segmentation algorithms on the measurement of (18)F-FDG PET texture parameters in non-small cell lung cancer. EJNMMI Res. 2017;7:60. doi:10.1186/s13550-017-0310-3.
18. Cook GJR, Azad G, Owczarczyk K, Siddique M, Goh V. Challenges and promises of PET radiomics. Int J Radiat Oncol Biol Phys. 2018;102(4):1083–9. doi: 10.1016/j.ijrobp.2017.12.268.
19. Ren CY, Zhang JP, Qi M, Zhang JG, Zhang YJ, Song SL, et al. Machine learning based on clinico-biological features integrated 18 F-FDG PET/CT radiomics for distinguishing squamous cell carcinoma from adenocarcinoma of lung. Eur J Nucl Med Mol Imaging. doi: 10.1007/s00259-020-05065-6.
20. Chang C, Zhou SH, Yu H, Zhao WL, Ge YQ, Duan SF, Wang R, Qian XH, Lei B, Wang LH, Liu L, Ruan MM, Yan H, Sun XY, Xie WH. A clinically practical radiomics-clinical combined model based on PET/CT data and nomogram predicts EGFR mutation in lung adenocarcinoma [J]. Eur Radiol, 2021, doi: 10.1007/s00330-020-07676-x.
21. Chang C, Sun XY, Wang G, Yu H, Zhao WL, Ge YQ, Duan SF, Qian XH, Wang R, Lei B, Wang LH, Liu L, Ruan MM ,YanH, Liu CY, Chen J, Xie WH. A machine learning model based on PET/CT radiomics and clinical characteristics predicts ALK rearrangement status in lung adenocarcinoma [J]. Frontiers in Oncology, 2021, 11: 603882, doi: 10.3389/fonc.2021.603882. eCollection 2021.

22. Liu HH, Zhang CY, Wang LJ, Luo R, Li JN, Zheng H, et al. MRI radiomics analysis for predicting preoperative synchronous distant metastasis in patients with rectal cancer. Eur Radiol, 2019, 29:4418-26. doi: 10.1007/s00330-018-5802-7.
23. Shu ZY, Shao Y, Xu YY, Ye Q, Cui SJ, Mao DW, et al. Radiomics nomogram based on MRI for predicting white matter hyperintensity progression in elderly adults. J Magn Reson Imaging. 2020;51:535-546. doi: 10.1002/jmri.26813.
24. Gibbs P, Turnbull LW. Textural analysis of contrast enhanced MR images of the breast. Magn Reson Med. 2003;50(1):92-98. doi: 10.1002/mrm.10496.
25. Collewet G, Strzelecki M, Mariette F. Influence of MRI acquisition protocols and image intensity normalization methods on texture classification. Magn Reson Imaging. 2004;22(1):81-91. doi: 10.1016/j.mri.2003.09.001.
26. Chung HH, Lee I, Kim HS, Kim JW, Park NH, Song YS, et al. Prognostic value of preoperative metabolic tumor volume measured by (1)(8)F-FDG PET/CT and MRI in patients with endometrial cancer. Gynecol Oncol. 2013;130:446-51. doi:10.1016/j.ygyno.2013.06.021.
27. Ouyang ML, Xia HW, Xu MM, Lin J, Wang LL, Zheng XW, et al. Prediction of occult lymph node metastasis using SUV, volumetric parameters and intratumoral heterogeneity of the primary tumor in T1-2N0M0 lung cancer patients staged by PET/CT. Ann Nucl Med. 2019;33:671-80. doi:10.1007/s12149-019-01375-4.
28. Boellaard R, Krak NC, Hoekstra OS, Lammertsma AA. Effects of noise, image resolution, and ROI definition on the accuracy of standard uptake values: a simulation study. J Nucl Med. 2004;45(9):1519-27.
29. J W Keyes Jr. SUV: standard uptake or silly useless value? J Nucl Med. 1995;36:1836-9.
30. Miyasaka Y, Suzuki K, Takamochi K, Matsunaga T, Oh S. The maximum standardized uptake value of fluorodeoxyglucose positron emission tomography of the primary tumour is a good predictor of pathological nodal involvement in clinical N0 non-small-cell lung cancer. Eur J Cardiothorac Surg. 2013;44:83-7. doi:10.1093/ejcts/ezs604.
31. Lee KH, Goo JM, Park SJ, Wi JY, Chung DH, Go H, et al. Correlation between the size of the solid component on thin-section CT and the invasive component on pathology in small lung adenocarcinomas manifesting as ground-glass nodules. J Thorac Oncol. 2014;9:74-82. doi:10.1097/JTO.0000000000000019.
32. Tsutani Y, Miyata Y, Nakayama H, Okumura S, Adachi S, Yoshimura M, et al. Prognostic significance of using solid versus whole tumor size on high-resolution computed tomography for predicting pathologic malignant grade of tumors in clinical stage IA lung adenocarcinoma: a multicenter study. J Thorac Cardiovasc Surg. 2012;143:607-12. doi:10.1016/j.jtcvs.2011.10.037.
33. Shiri I, Rahmim A, Ghaffarian P, Geramifar P, Abdollahi H, Bitarafan-Rajabi A. The impact of image reconstruction settings on 18F-FDG PET radiomic features: multi-scanner phantom and patient studies. Eur Radiol. 2017;27:4498-509. doi:10.1007/s00330-017-4859-z.

34. van Velden FH, Kramer GM, Frings V, Nissen IA, Mulder ER, de Langen AJ, et al. Repeatability of Radiomic Features in Non-Small-Cell Lung Cancer [(18)F]FDG-PET/CT Studies: Impact of Reconstruction and Delineation. Mol Imaging Biol. 2016;18:788-95. doi:10.1007/s11307-016-0940-2.

Figures

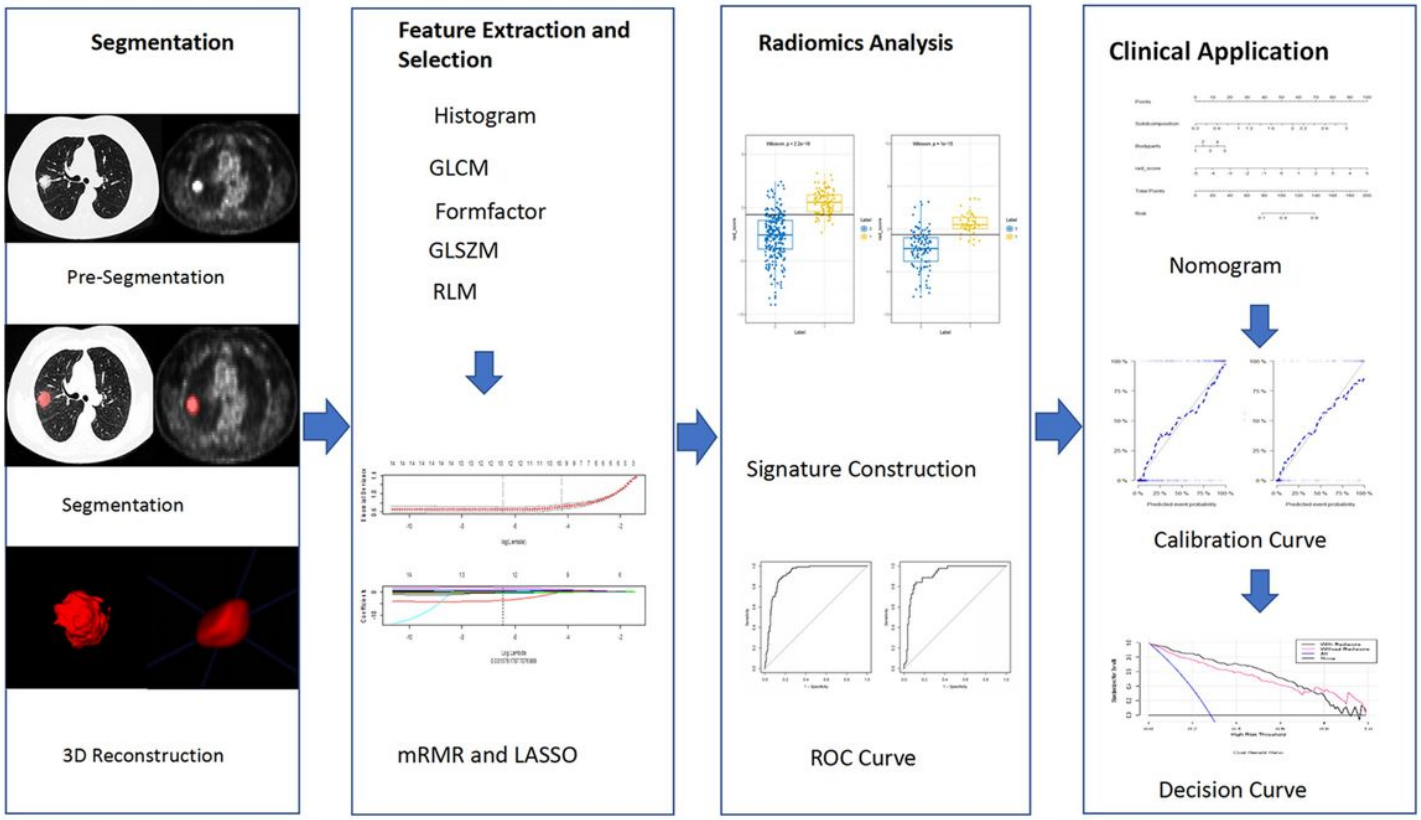

Figure 1

The workflow of developing a radiomic model based on PET/CT images to predict LLNM of lung adenocarcinoma.

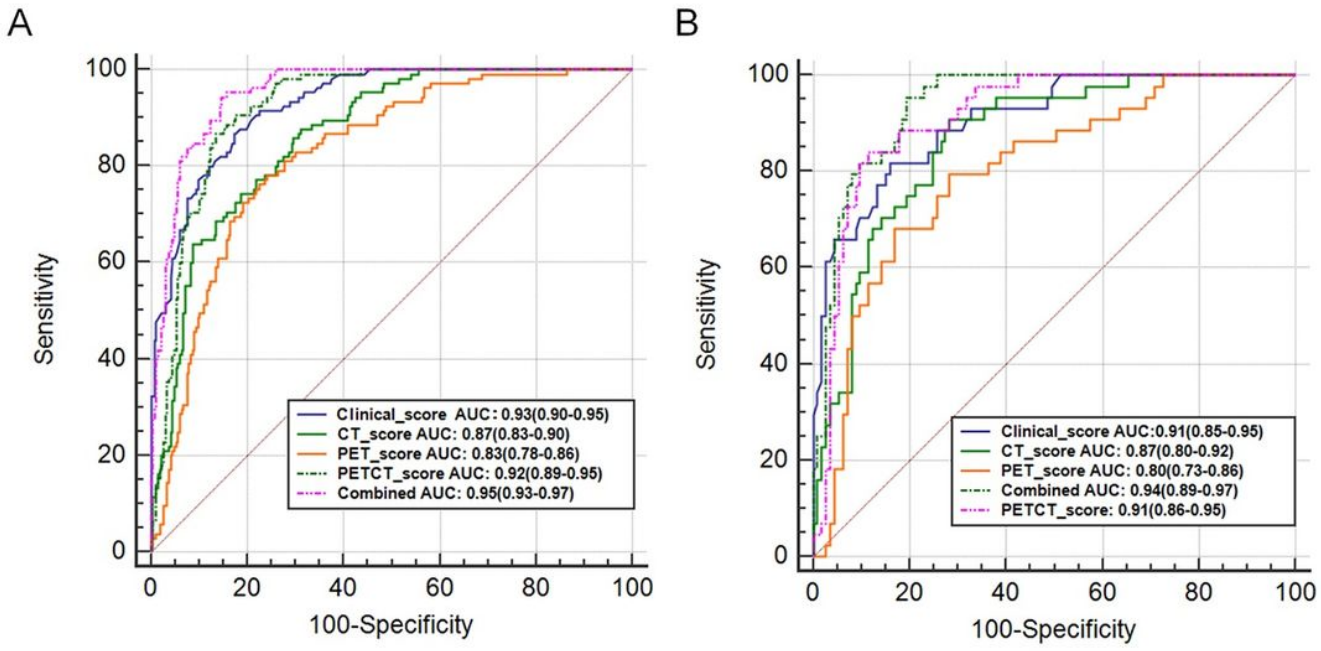

Figure 2

ROC curve analysis of five predictive models, including clinical model, CT radiomic model, PET radiomic model, PET/CT radiomic model, and combined PET/CT radiomic-clinical model in the training group (A) and test group (B), respectively.

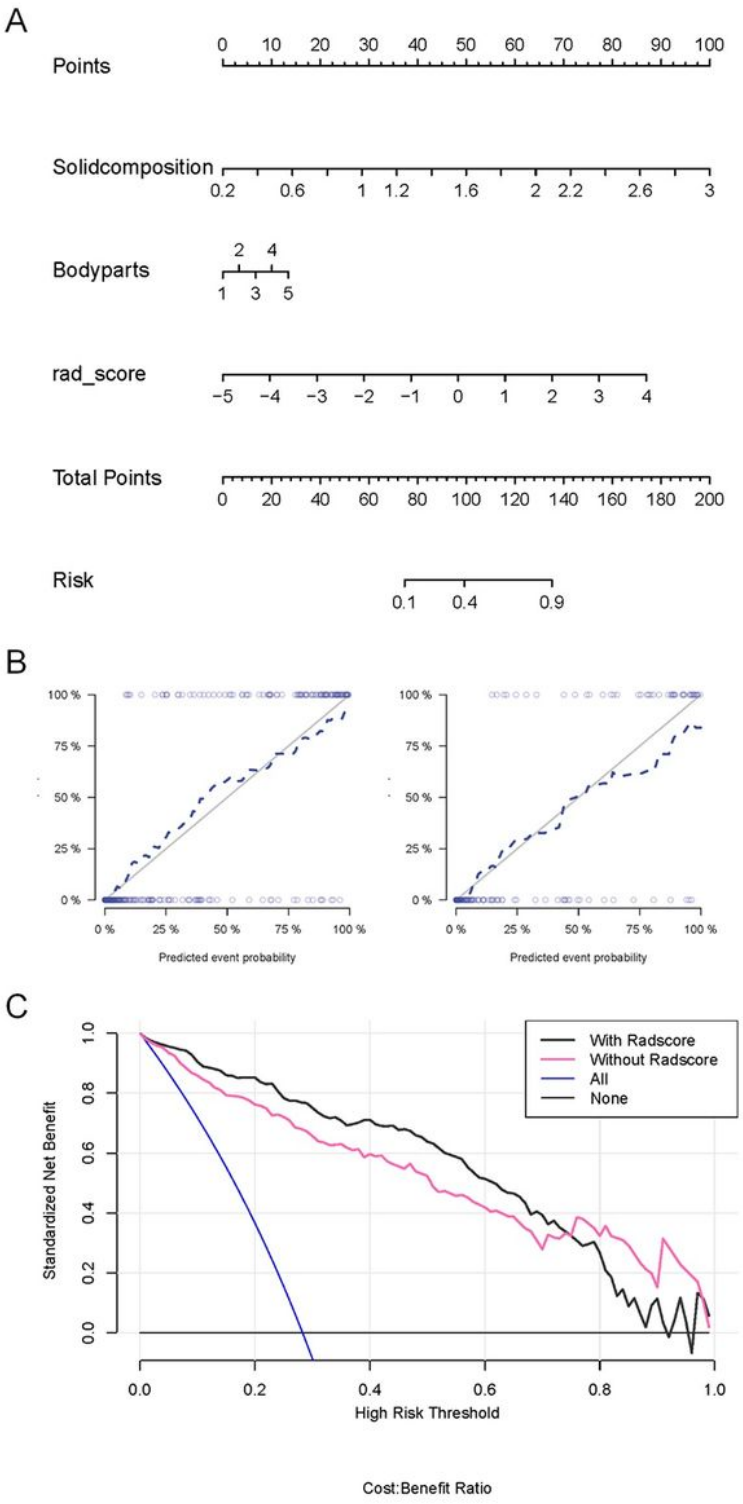

Figure 3

Evaluates the performances of the integrated PET/CT molecular radiomics-clinical model. (A) The nomogram was developed by combining the PET/CT radiomic score and the clinical features of the solid composition and location/body part (1, 2, 3, 4, 5 respectively represent the upper lobe, middle lobe, and lower lobe of the right lung, upper lobe and lower lobe of the left lung). (B) Calibration curve with Hosmer-Lemeshow test of the nomogram in the training cohort (left panel) and test cohort (right panel). The

calibration curve shows the calibration of the model in terms of consistency between the predicated risk of LLNM and real observed LLNM status. The x-axis represents the predicted risk of LLNM and the y-axis represents the real LLNM status. (C) Decision curve analysis for the nomograms. The y-axis measures the standardized net benefit. The dark line represents the PET/CT radiomics and clinical features nomogram model, the red line represents the clinical features nomogram, the gray line represents the assumption that all patients are negative for LLNM and the blue line represents the assumption that all patients are positive for LLNM.

Supplementary Files

This is a list of supplementary files associated with this preprint. Click to download.

- SupplementaryFigureLegends.doc
- SupplementaryFigureS1.tif
- SupplementaryFigureS2.tif
- SupplementaryFigureS3.tif
- SupplementaryFigureS4.tif
- SupplementaryMethods.docx
- SupplementaryTableS1.docx